RESEARCH

Neuronal guanine nucleotide exchange factor promotes the axonal growth and cancer cell proliferation via Ephrin-A3/EphA2 axis in lung adenocarcinoma

Jie Mi[1†], Wentian Zhang[1†], Yijiu Ren[1†], Lei Zhu[1], Bei Yang[1*], Hao Wang[1*] and Liang Duan[1*]

Abstract

Background   Neural infiltration has been found in various cancers and the infiltrating nerves influence tumor growth and dissemination. In non-small cell lung cancer, pan-neuronal marker PGP9.5 was detected by immunohistochemical staining and its high expression correlated with poor prognosis. However, the existence of nerve fibers and the mechanism driving neural infiltration remains unclear.

Method   We first used immunohistochemical staining to assess the density of nerve fibers in patients with lung adenocarcinoma of different tumor sizes. Following that, we performed differential expression analysis and univariate Cox prognostic analysis, using public datasets and cell experiments to identify the gene that triggers neural infiltration and is associated with cancer progression and unfavorable prognosis. Finally, molecular biology experiments and a subcutaneous tumor model were used to deeply analyze the mechanism that the gene regulates neural infiltration and tumor progression.

Results   In lung adenocarcinoma patients, the density of PGP9.5 positive nerve fibers within tumors larger than 2 cm in diameter is significantly higher than that in tumors smaller than 2 cm. Bioinformatics analysis suggested NGEF, KIF4A, and PABPC1 could be the genes that trigger neural infiltration and are associated with cancer progression and unfavorable prognosis. Subsequent co-culture experiments with neurons showed that the increased expression of NGEF in lung cancer cells significantly enhanced axonal growth in neurons. Meanwhile, GSE30219 datasets indicated that patients exhibiting high levels of NGEF expression are associated with larger tumor sizes, higher lymph node involvement, and reduced overall survival rates. At the level of molecular mechanisms, the knockdown of Ephrin-A3 in ND7/23 neurons or the use of ALW-II-41-27 resulted in a significant decrease in neurite outgrowth when co-cultured

[†]Jie Mi, Wentian Zhang and Yijiu Ren contributed equally to this work.

*Correspondence:
Bei Yang
iori2335@163.com
Hao Wang
yaoyao4345@163.com
Liang Duan
duan-liang@163.com

Full list of author information is available at the end of the article

Mi *et al. Journal of Translational Medicine*   (2025) 23:246

Page 2 of 14

with LA795 cells. In animal model, NGEF overexpression significantly promoted tumor growth and increased the density of nerve fibers, and these effects were inhibited by ALW-II-41-27.

Conclusions NGEF facilitates the infiltration of nerve and the growth of cancer cells in lung adenocarcinoma through the Ephrin-A3/EphA2 pathway, suggesting that NGEF is a promising target for disrupting interactions between nerves and tumors. Biomaterials that focus on NGEF are anticipated to be a potential treatment option for lung cancer.

Keywords NGEF, Axonal growth, Lung adenocarcinoma, Ephrin-A3, EphA2

Introduction

Non-small cell lung cancer is a major contributor to cancer-related deaths globally, with lung adenocarcinoma is the main pathological subtype of non-small cell lung cancer [1, 2]. Despite advancements in lung cancer treatment, overall survival rates remain low, partly due to that some lung adenocarcinomas are detected at advanced stages. Therefore, elucidating the mechanisms that regulate lung adenocarcinoma progression is crucial for improving patient outcomes and creating innovative therapies [3].

Recent studies have identified neurogenesis as a novel characteristic of cancer. The presence of nerve fibers in tumors has been linked to unfavorable clinical outcomes in various types of cancer, such as lung adenocarcinoma [4], colorectal cancer [5], pancreatic cancer [6], and prostate cancer [7]. A study by Shao et al. found that, in human lung adenocarcinoma samples, sympathetic fibers tended to be more abundant in the surrounding area of the tumor, while parasympathetic fibers were primarily found within the tumor itself [4]. The density of these fibers was associated with a higher risk of recurrence in lung cancer patients. Elevated levels of neuronal markers have also been linked to reduced survival and increased metastasis in lung cancer [8, 9]. The nervous system's influence on tumor growth, metastasis, and immune response underscores the importance of investigating the molecular mechanisms underlying neurogenesis in lung adenocarcinoma [10–12]. Understanding these mechanisms could lead to advancements in controlling tumor progression and improving therapeutic outcomes for patients.

Currently, there is a paucity of research examining the presence of nerve fibers in lung cancer [4, 13]. Consequently, we first identified the existence of PGP9.5-immunopositive nerve fibers in lung adenocarcinoma using clinical specimens, revealing a positive correlation between tumor size and nerve fiber density. Afterwards, we conducted bioinformatics analysis to identify the differentially expressed genes (DEGs), axonal growth-related genes, and prognostic-related genes. The genes that overlapped in these categories were identified as KIF4A, NGEF, and PABPC1. Following comparisons of in vitro experiments and validation in GSE30219 dataset, we selected NGEF for further investigation. By

conducting a protein-protein interaction (PPI) analysis and in vitro experiments, we discovered that NGEF may promote axonal growth via the Ephrin-A3/EphA2 signaling axis. Finally, we confirmed the involvement of NGEF and Ephrin-A3/EphA2 signaling axis in enhancing axonal growth and cancer cell proliferation in lung adenocarcinoma using a subcutaneous tumor formation model.

Materials and methods

Human tissue samples

Lung tumor samples were collected from patients with lung adenocarcinoma (LUAD) between May 20 and May 30, 2024, following the provision of informed consent and approval from the ethics committee of Shanghai Pulmonary Hospital Affiliated Tongji University (approval no: K21-111Y). The inclusion criteria consist of single solid or mixed solid nodules measuring between 1 and 4 cm in diameter, along with a pathological diagnosis of lung adenocarcinoma. The exclusion criteria involve patients who have undergone neoadjuvant therapy or those with lymph node or distant metastasis. None of the patients received radiotherapy or chemotherapy before surgery. The staging of tumors was conducted by pathologists who are experienced and certified by the board. The staging and supplementary subject-specific information are available in Supplementary tables. S1.

Public data acquisition and processing

Gene expression and clinical data for lung adenocarcinoma were obtained from TCGA database (https://portal.gdc.cancer.gov/, accessed on October 20, 2023), while the gene expression matrix and clinical information for GSE were sourced from the Gene Expression Omnibus (GEO) database (http://www.ncbi.nlm.nih.gov/geo/, accessed on October 20, 2023). Only LUAD patients with full survival information, pathological results and essential clinical data were included in this study. The expression levels of KIF4A, NGEF, and PABPC1 in lung adenocarcinoma were validated by querying the Human Protein Atlas database (HPA, http://www.proteinatlas.org/). To identify the gene sets associated with axonal growth, a search was performed using the keyword "axon" and species "Homo sapiens" in the Gene Set Enrichment Analysis (GSEA) database within the Molecular Signatures Database (MSigDB) (https://www.gsea

msigdb.org/gsea/msigdb/index.jsp) [14]. Subsequently, genes linked to axonal growth, regeneration, or development were all extracted and integrated, resulting in the identification of 860 axonal growth-related genes (Supplementary tables S2).

DEGs and prognostic gene analysis

The data was subjected to standardized preprocessing and log transformation utilizing appropriate R packages. DEGs between normal and tumor samples from TCGA were identified as those exhibiting a log2 fold change greater than 1 and a false discovery rate less than 0.05. Univariate Cox analysis was performed using the overall survival data of TCGA patients, and prognostic genes were identified based on a significance level of $P < 0.05$ [15]. The intersection of DEGs, prognostic genes, and axonal growth-related genes was visualized using the E Venn website (http://www.ehbio.com/test/venn/#/). Furthermore, PPI network was established using the STRING database (https://string-db.org/) to investigate potential pathways associated with the gene of interest [16]. Levels of NGEF expression of lung adenocarcinoma patients were compared among different T stages, N stages and M stages [17].

In vitro neurite outgrowth with lung adenocarcinoma cells

The LA795 lung adenocarcinoma cell line and ND7/23 cells, a hybridoma of neonatal rat DRG neurons and mouse neuroblastoma cells N18TG2, were procured from the Cell Bank of the Chinese Academy of Sciences in Shanghai, China. In the co-culture setup, ND7/23 cells were initially seeded at a concentration of 12,000 cells/mL and maintained in minimum essential medium α (MEM, Gibco™, Cat#11900073) supplemented with 10% fetal bovine serum (FBS, Gibco™, Cat#10099158), 1% penicillin-streptomycin (Gibco™, Cat#15070063), and 1% L-glutamine (Gibco™, Cat#25030149) overnight [18]. Subsequently, the medium was replaced with MEM containing 2% FBS, 1% penicillin-streptomycin, and 1% L-glutamine, and LA795 cells were added at a density of 5000 cells/mL. Following a 24-hour co-culture period, the cells were fixed in 4% paraformaldehyde (Sigma-Aldrich, Cat#158127) in phosphate-buffered saline (PBS) at 4 °C for 20 min and then rinsed twice with PBS. Subsequently, the cells were permeabilized using a blocking buffer comprising 5% bovine serum albumin (BSA) (Sigma-Aldrich, Cat#B2064) and 0.1% Triton X-100 (Sigma-Aldrich, Cat#T8787) in PBS for 1 h at room temperature. The cells were then stained with primary antibody (β-tubulin-III, Cat#66375-1-Ig, 1:300, BioTalentum Ltd) and CY3 labeled secondary antibody (Cat#GB21303, 1:100, BioTalentum Ltd) and DAPI (Sigma-Aldrich, Cat#D8417-1MG), followed by two washes with blocking buffer. Fluorescence and bright-field images were acquired using a fluorescent microscope (Leica Q500MC, Leica, Germany). Neurite length was quantified using Image J software, and statistical analysis was conducted using One-Way ANOVA to assess significance [19].

Transfection of cells with plasmids and transduction of cells with lentivirus

For the overexpression of NGEF, KIF4A, and PABPC1, plasmid vectors packaging was facilitated by OBiO Technology (Shanghai) Corp, Ltd. The complete gene sequences (Supplementary tables) were integrated into the pCDNA3.1 (+)-P2A-GFP plasmid. Cells were cultured at 60% confluency for transfection, utilizing Lipofectamine 2000 reagent (Thermo Fisher, Cat#11668019) as per the manufacturer's instructions. Lentiviral vectors (Thermo Fisher, GeneAssist™ Custom siRNA Builder) were designed to silence EphrinA3 in ND7/23 cells, which were divided into distinct groups: non-targeting control (NTC) group, siEphrinA3#1 group, siEphrinA3#2 group, and siEphrinA3#3 group. Transfection procedures were carried out in accordance with the lentiviral instructions. Post-transfection, verification of transfection was conducted through western blot and quantitative polymerase chain reaction (qPCR), followed by selection of stably transfected cell lines for subsequent experiments [20].

Immunohistochemical and immunofluorescent staining

Tumors were preserved in 4% paraformaldehyde solution overnight and subsequently processed into paraffin sections using conventional methods. Immunohistochemical and immunofluorescent staining procedures were conducted according to established protocols, involving deparaffinization, antigen retrieval, and incubation with primary and secondary antibodies [21]. Negative controls were included in the experiments, wherein the primary antibody was replaced with IgG-matched controls while following the same protocols. The immunohistochemical outcomes were evaluated through semi-quantitative analysis, which involved integrating the percentage of positive cells. The primary antibodies used in the study were as follows: PGP9.5 (Cat#ab108986, 1:300, Abcam) and Ki67 (Cat#ab279653, 1:50, Abcam). In order to conduct a semiquantitative analysis of nerve fibers labeled with PGP9.5, the positive areas were quantified at four standard high-powered fields within each section. The outcome was then expressed as a percentage of the total area. Similarly, for the semiquantitative analysis of Ki67 positive cells, the counts of positive cells and total cells were recorded at four standard high-powered fields within each section, with the final result presented as a percentage of total cells. The data were averaged by two impartial investigators who were unaware of the sample grouping [21, 22].

Mi *et al. Journal of Translational Medicine*   (2025) 23:246

Page 4 of 14

RT-qPCR

The cellular RNA was isolated using an RNA kit (Cat#a15596026; Invitrogen), followed by assessment of its concentration and purity. Subsequently, the RNA was reverse transcribed into cDNA utilizing the Prime-Script RT Reagent Kit (Takara, DaLian, China) as per the provided guidelines. RT-qPCR analysis was conducted using the RT-qPCR kit following the manufacturer's protocol, with GAPDH utilized as an internal control [22]. The primer sequences can be found in the Supplementary tables (S4).

Western blot and co-immunoprecipitation

The cultured cells or tissues were subjected to protein extraction using RIPA buffer (Cat# 89901, Thermo Scientific™) supplemented with phenylmethylsulfonyl fluoride (Cat# 36978, Thermo Scientific™) and a protein phosphatase inhibitor cocktail (Cat# 78420, Thermo Scientific™). The protein concentration was determined using a BCA Protein Assay Kit (Cat#A65453, Pierce™ BCA Protein Assay Kits), and approximately 50 µg of total protein was loaded onto a 10% sodium dodecyl sulfate-polyacrylamide gel electrophoresis. The separated proteins were then transferred to a polyvinylidene fluoride (PVDF) membrane following a previously established protocol. Subsequently, the PVDF membranes were blocked with 5% BSA for 2 h and then incubated overnight at 4 °C with primary antibodies targeting specific proteins and GAPDH. Following incubation, the membranes were washed with Tris-buffered saline (TBS-T), incubated with secondary antibodies, and subjected to further washing steps. The protein bands were scanned, and semi-quantitative analysis was conducted by measuring integrated density using Image-J software [21].

For co-immunoprecipitation experiments, the protein samples containing phenylmethylsulfonyl fluoride were incubated with primary antibodies on a rocking platform at 4 °C for 12 h. Protein A/G beads were then added to the immunoprecipitation reaction mixture and incubated on a rocking platform at 4 °C for an additional 12 h. The bound proteins were eluted using loading buffer and analyzed by SDS-PAGE. Following three washes with PBS containing protein inhibitors, the immunoprecipitated proteins were subjected to western blotting using a GPX4 antibody for analysis [23].

Transplantation tumor model

A group of 6-week-old male BALB/c nude mice was obtained from a biotech company (Shanghai JieSiJie Laboratory Animal Co.,Ltd.) for the purpose of establishing a tumor transplantation model. The mice were housed in a pathogen-free environment and handled in compliance with established protocols and regulations concerning animal welfare. Cultured cells were collected, suspended in PBS, and subsequently injected subcutaneously into the middle posterior region of the armpit of the BALB/c nude mice at a concentration of 1×10^6 cells in 100 uL. Upon the development of visible tumors, their size was monitored weekly using micrometer calipers. Tumor volumes were determined using the formula: volume = 0.5a $\times$ b^2, where 'a' and 'b' denote the larger and smaller tumor diameters, respectively. Following a 4-week period, the mice were euthanized, and the primary tumors were excised, weighed, fixed in a 10% formalin solution, and embedded in paraffin. The establishment of animal models and methodologies for measuring tumor-related parameters is derived from previously published study [23]. All animal experimentation procedures were subjected to review and approval by Bestcell Model Biological Center (BSMS 2024-01-22 A).

ELISA

The total protein content of tumor tissue from mice was extracted and quantified using the BCA method. The concentration of PGP9.5 was assessed using an ELISA kit (Cat# MBS2516002, MyBioSource) and subsequently adjusted relative to the total protein levels according to our previous published study [22].

Statistical analysis

All data were expressed as the mean ± SD. Unpaired Student's *t* test (two-tailed), or one-way ANOVA with *Tukey's* post hoc tests, or two-way ANOVA with *Bonferroni* post hoc tests were separately used in different experiments as indicated in the figure legend. GraphPad Prism (version 7.00) and R was used for statistical analysis.

Results

Human lung adenocarcinoma is infiltrated by nerve fibers

Previous studies have demonstrated the existence of nerve fibers in lung cancer tissues. In order to further verify this phenomenon, we procured clinical samples of lung cancer and quantified the density of nerve fibers using IHC staining targeting the neuronal marker PGP9.5. Figure 1 provides a detailed presentation of the IHC staining outcomes for two distinct lung adenocarcinomas patients varying in size. Specifically, Fig. 1A displays the chest computed tomography (CT) image of lung adenocarcinoma patient A with a tumor measuring 1.8 cm, while Fig. 1B and C depict the corresponding IHC findings for patient A. Figure 1D illustrates another lung adenocarcinoma case patient B, whose tumor size was 3 cm, with Fig. 1E and F showcasing his IHC result. To ensure the accuracy of the findings, negative controls were utilized and presented. The IHC results indicate a higher presence of nerve fibers in patients with larger
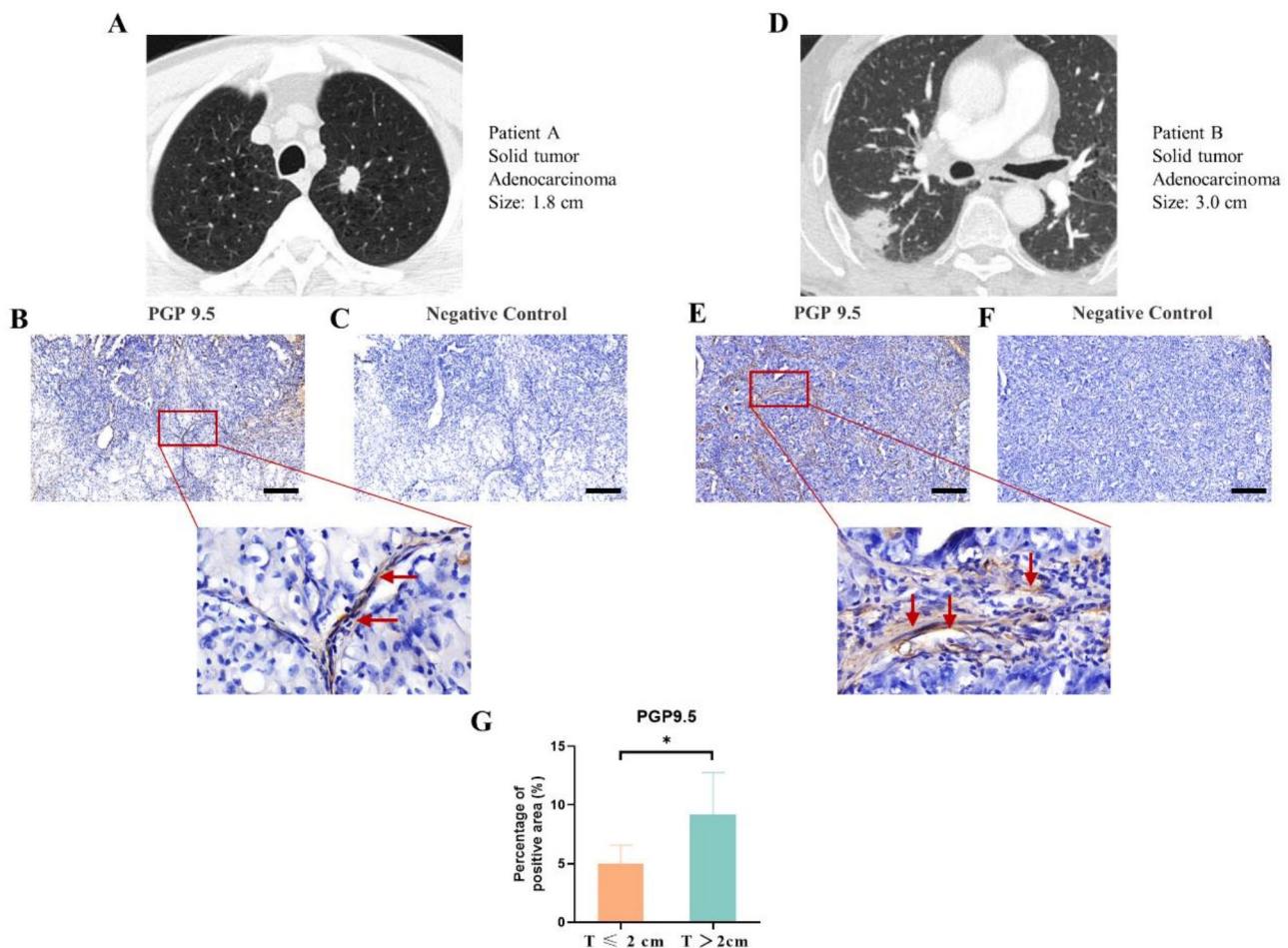
Fig. 1 Human lung adenocarcinoma is infiltrated by nerve fibers. (**A**) Chest CT scan of LUAD patient A with solid tumor size as 1.8 cm. (**B-C**) PGP 9.5 staining in patient A with negative control. (**D**) Chest CT scan of LUAD patient B with solid tumor size as 3 cm. (E-F) PGP 9.5 staining in patient B with negative control. (**G**) Semiquantitative results of IHC staining. Unpaired Student's *t* test. $n = 7$ in T ≤ 2 cm group and $n = 8$ in T >2 cm group. Scale bar: 200 μm. *$P < 0.05$

tumors ($P < 0.05$, Fig. 1.G), predominantly located within the tumor stroma.

Identification of axonal growth-related genes that are differentially expressed and have prognostic value using TCGA data

We identified the genes that regulate axonal growth in lung adenocarcinoma by conducting differential expression analysis and univariate Cox analysis, followed by intersecting these results with axonal growth-related genes (Fig. 2.A). A total of 489 TCGA-LUAD patients and 53 adjunct nontumor samples were included in the analysis. The differential expression analysis and subsequent intersection with axonal growth-related gene set revealed that 159 axonal growth-related genes exhibited differential expression between tumor samples and adjunct non-tumor samples. The univariate Cox analysis identified 476 genes with prognostic significance. From the intersection of these results, three genes - KIF4A, NGEF,

and PABPC1 - were identified (Fig. 2.B). Survival curves indicated that these genes possessed favorable prognostic values (Fig. 2.C). To further assess the expression levels of the corresponding proteins of these genes, IHC results from the HPA database were obtained, revealing that these genes were overexpressed in tumor samples compared to normal tissue (Fig. 2.D).

NGEF demonstrated an increased ability to promote axonal growth in a co-culture system

To further investigate the genes that promote nerve fiber growth in lung adenocarcinoma, NGEF, KIF4A, and PABPC1 were individually overexpressed in LA795 cells and subsequently co-cultured with ND7/23 neurons. The results depicted in Fig. 3A-C indicate that the mRNA levels of NGEF, KIF4A, and PABPC1 were elevated by approximately 15, 20, and 15-fold, respectively. Live cell imaging revealed that the presence of overexpressed LA795 cells enhanced the neurite outgrowth of ND7/23
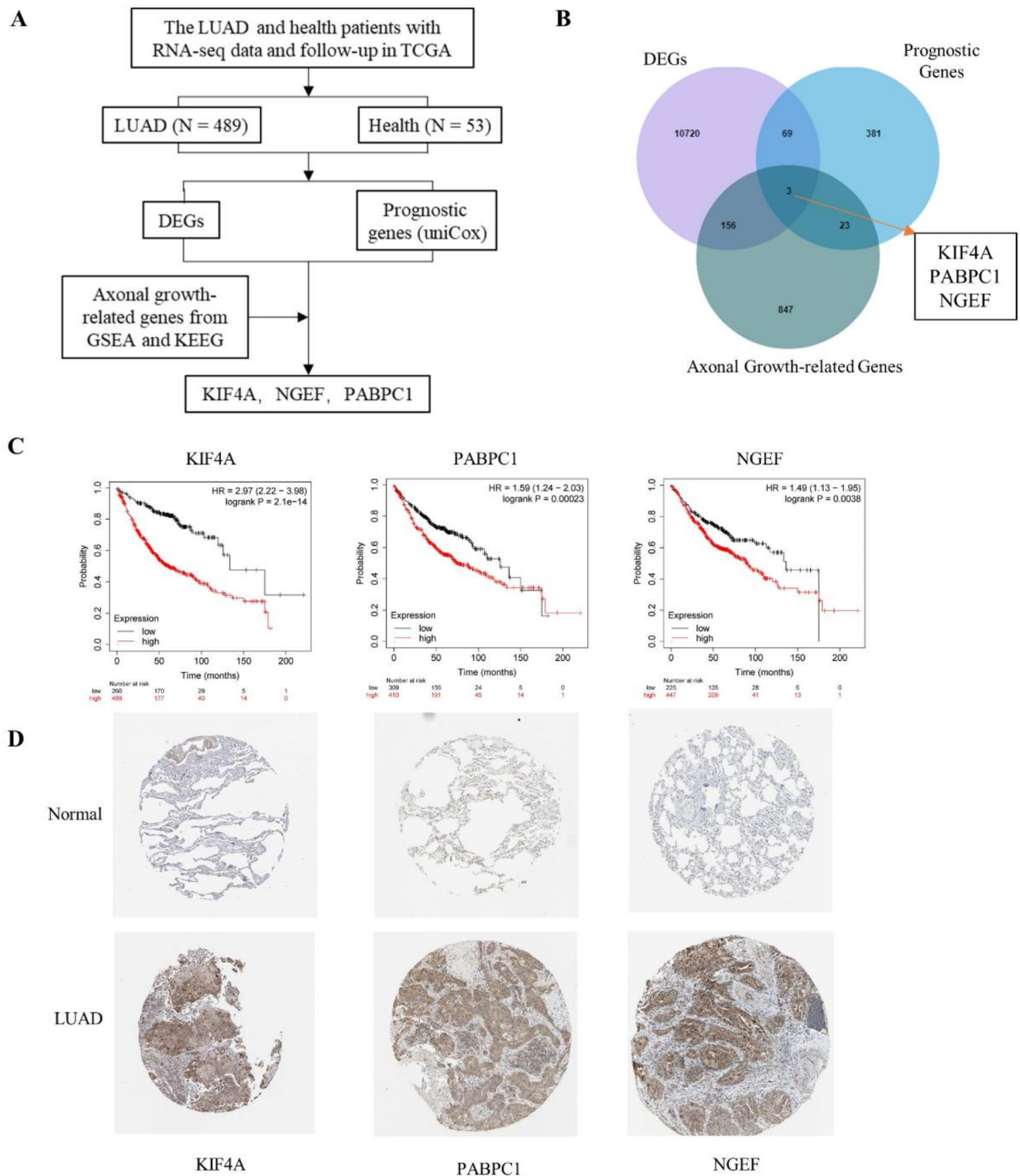
Fig. 2 Screening the genes regulating axonal growth in lung adenocarcinoma (**A**) Flow chart for screening genes of interest. (**B**) Venn of DEGs, axonal growth-related genes and prognostics genes. (**C**) Survival curves for the three genes. (**D**) Immunohistochemical results of the protein expressed in normal and tumor tissues
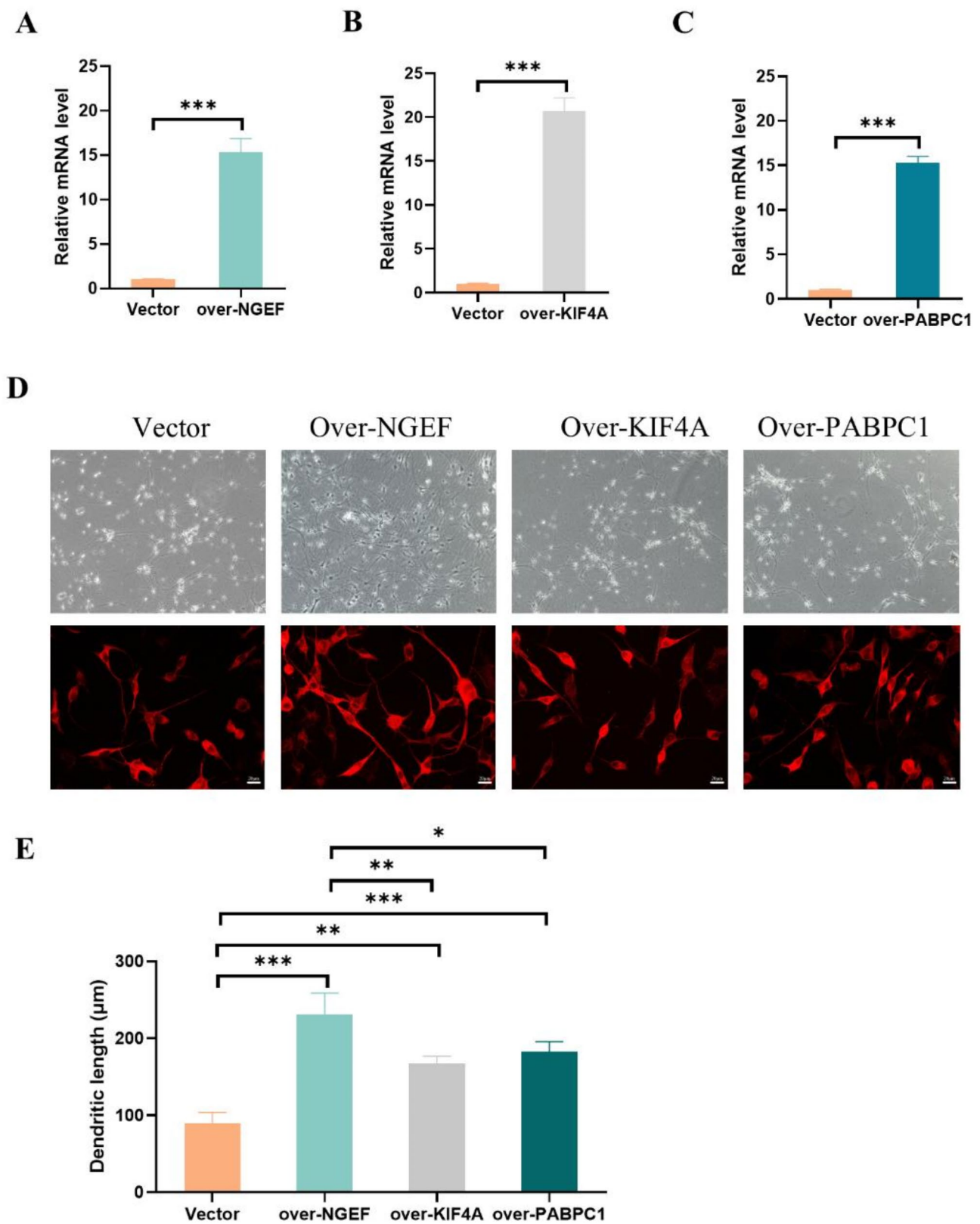
Fig. 3 NGEF promoted the axonal growth when coculture with cancer cells. (**A**-**C**) mRNA level after gene overexpression. Student's *t* test, ***$P < 0.001$. (**D**) Live cell imaging and β-tubulin III staining of neurons. Scale bar: 20 μm. (**E**) Dendritic length between groups. One-way ANOVA, *$P < 0.05$, ** $P < 0.01$, ***$P < 0.001$

cells, with NGEF overexpression showing the most significant impact on axonal growth in neurons. Subsequently, to visualize neurite growth at higher resolutions, the cell cultures were fixed and stained with β-tubulin III. The findings demonstrated that both NGEF, KIF4A, and PABPC1 promoted the axonal growth in neurons, with NGEF exhibiting the most robust effect (Fig. 3D and E). Consequently, NGEF was selected for further in vitro and in vivo investigations.

Increased NGEF expression correlated with clinical parameters

Human lung cancer samples showed a direct relationship between tumor size and nerve fiber density. Subsequently, we explored the connection between NGEF expression and the clinical characteristics of lung cancer patients. Analysis of TCGA-LUAD data revealed that NGEF was significantly upregulated in tumor tissue compared to normal tissue (Fig. 4A). Moreover, NGEF expression levels were found to be positively associated
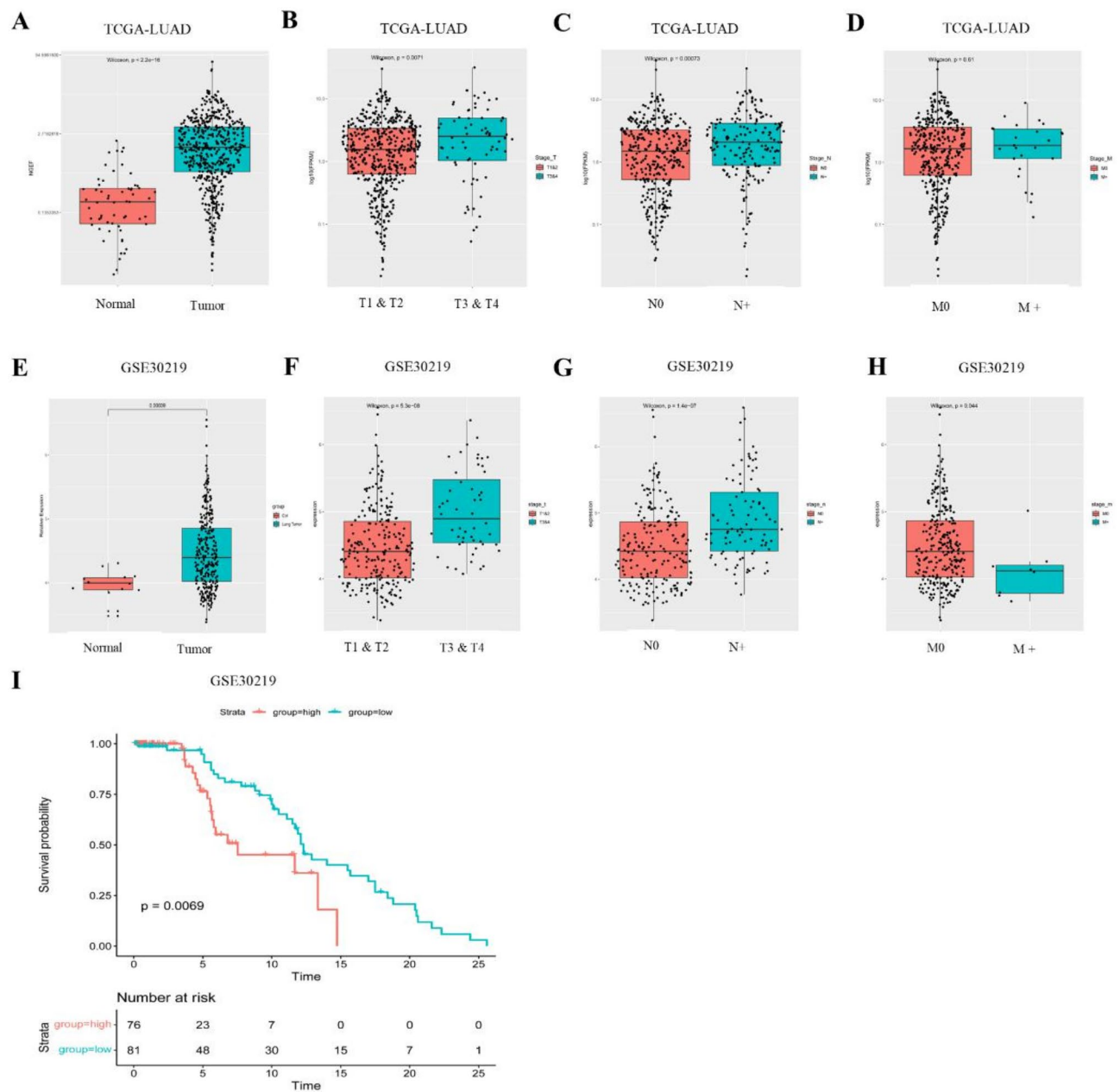

Fig. 4 Increased NGEF expression correlated with clinical parameters. (**A**) NGEF expression level in LUAD-TCGA dataset. (**B-D**) The NGEF expression level in LUAD-TCGA dataset between different tumor size, lymph node involvement and distant metastasis. (**E**) NGEF expression level in GSE30219. (**F-H**) The NGEF expression level in GSE30219 between different tumor size, lymph node involvement and distant metastasis. (**I**) Survival curve for NGEF in GSE30219

with larger tumor size (Fig. 4B) and lymph node involvement (Fig. 4C). However, no statistically significant correlation was observed with different metastasis stages (Fig. 4D). These results were further validated using the GSE30219 dataset, where NGEF expression levels were elevated in LUAD patients compared to controls in GSE31210 dataset (Fig. 4E). Higher NGEF expression was also linked to larger tumor size (Fig. 4F) and lymph node metastasis (Fig. 4G), but not distant metastasis (Fig. 4H). Additionally, Kaplan-Meier survival analysis indicated that individuals with high NGEF expression levels had a shorter overall survival compared to those with low NGEF expression levels in LUAD patients from GSE30219 (Fig. 4I). Thus, the findings suggest that increased NGEF expression is associated with the clinical parameters of lung adenocarcinoma.

Ephrin-A3/EphA2 axis facilitated NGEF to promote the growth of neuron extensions

The PPI analysis conducted on the STRING database revealed that NGEF predominantly interacts with EphA, with NGEF acting as the ligand for Eph receptors (Fig. 5A). This suggests the involvement of the Ephrin-A/EphA axis in NGEF-mediated neurite outgrowth in neurons. To investigate this further, we conducted a qPCR screening to identify the Ephrin-A subtype in ND7/23 cells and the EphA subtype in LA795 neurons. Our findings indicated that Ephrin-A3 was notably expressed in ND7/23 neurons (Fig. 5B), while EphA2 exhibited highest expression levels in LA795 cells (Fig. 5C). Subsequent western blot analysis confirmed the expression of EphrinA3 in ND7/23 neurons and EphA2 in LA795 cells (Fig. 5D). Additionally, co-immunoprecipitation (Co-IP) analysis of protein extracts from ND7/23 and LA795 co-culture demonstrated the co-precipitation of NGEF with EphA2 (Fig. 5E) and EphA2 with EphrinA3 (Fig. 5F). To elucidate the significance of EhprinA3, we generated stable EphrinA3 knockdown (KD) cell models in ND7/23 neurons (siEphrinA3 #1, siEphrinA3 #2, and siEphrinA3 #3). Notably, siEphrinA3 #3 exhibited a significant reduction in the transcriptional and protein levels of EhprinA3 and was subsequently utilized in subsequent experiments (Fig. 5G&H). To further confirm the involvement of the Ephrin-A/EphA axis in NGEF-mediated neurite outgrowth in neurons, we co-cultured ND7/23 cells with EphrinA3 gene knockout LA795 cells or treated the co-culture system of ND7/23 cells and LA795 cells with ALW-II-41-27, a novel Eph receptor tyrosine kinase inhibitor. Immunofluorescence images and semi-quantitative statistical analysis revealed that siEphrinA3 and ALW-II-41-27 significantly inhibited the dendritic length of ND7/23 neurons after 24 h of co-culturing with LA795 cells (Fig. 5I&J). These results underscore the critical role of the Ephrin-A3/EphA2 axis in NGEF-mediated neuronal outgrowth.

NGEF overexpression promotes the growth of tumor and nerve fibers

In the subcutaneous tumor formation model, initial observations revealed challenges in detecting nerve fibers within tumors using IHC under normal conditions. Therefore, NGEF overexpression was employed instead of a knockout method to investigate the stimulatory impact of NGEF on nerve fiber growth and tumor proliferation in lung adenocarcinoma. The mice were randomly allocated into three groups: vector group, over-NGEF group and over-NGEF + ALW-II-41-27 group (Fig 6 A). At the third and fourth week, the tumor volume in over-NGEF group was significantly larger as compared to vector group and over-NGEF + ALW-II-41-27 group (Fig.6B). Additionally, at the fourth week, vector group has larger tumor volume than over-NGEF + ALW-II-41-27 group (Fig.6B). Furthermore, over-NGEF group has significant higher tumor weight as compared to vector group and over-NGEF + ALW-II-41-27 group (Fig. 6C). Western blot results verified the elevated NGEF protein levels in the over-NGEF group and over-NGEF + ALW-II-41-27 group as compared to the vector group (Fig. 6D&E). The IHC staining indicated that over-NGEF group has a significant higher Ki67 positive rate within the tumor tissue as compared to other two groups (Fig. 6.F&G). Regarding nerve fiber density, IHC findings indicated a greater presence of PGP 9.5 positive regions (red arrow in the figure) in over-NGEF group as compared to vector group (Fig. 6H&I). Moreover, PGP9.5 content in tumor tissues was quantified using ELISA, revealing a significant increase in PGP9.5 content in over-NGEF group as compared to vector group and over-NGEF + ALW-II-41-27 group (Fig. 6J). Collectively, these findings consistently support the notion that NGEF plays a critical role in the axonal growth and tumor progression in lung adenocarcinoma and Ephrin-A3/EphA2 axis mediate the NGEF induced axonal growth and tumor cell proliferation (Fig. 6K).

Discussion

This study initially identified three genes, namely NGEF, KIF4A, and PABPC1, as potential contributors to the nerve fiber growth in LUAD based on clinical samples. Following a bioinformatics analysis, NGEF was singled out as the primary focus of investigation. Subsequent in vitro neuron and tumor co-culture experiments confirmed NGEF's significance. Further in vivo and in vitro investigations revealed that NGEF facilitates nerve fiber growth and tumor cell proliferation in lung adenocarcinoma via Ephrin-A3/EphA2 axis.
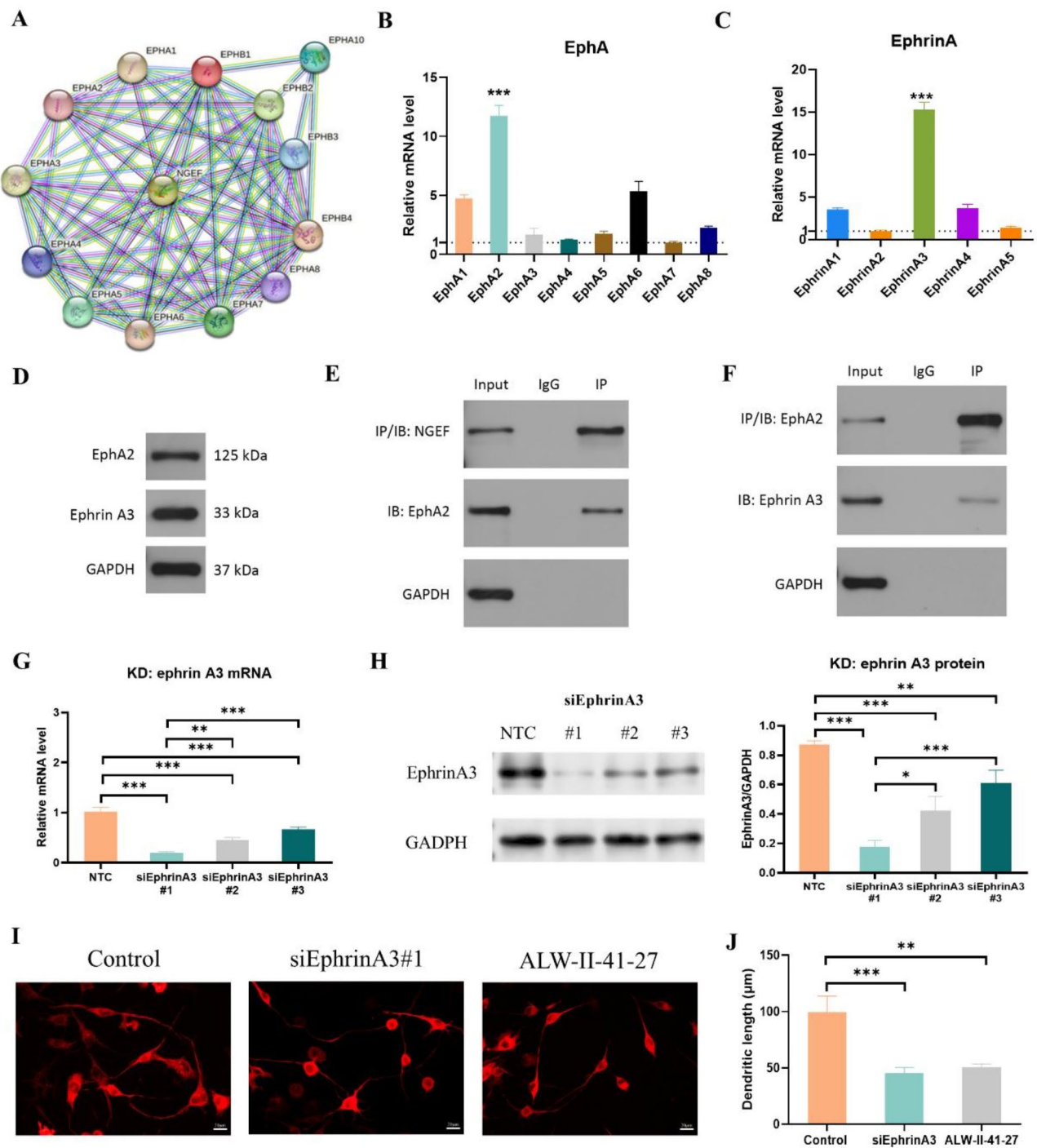
Fig. 5 Ephrin-A3/EphA2 axis facilitated NGEF to promote axonal growth. (**A**) PPI analysis. (**B**) mRNA level of different EphA subtypes. One-way ANOVA. ***$P < 0.001$. (**C**) mRNA level of different Ephrin-A subtypes. One-way ANOVA. ***$P < 0.001$. (**D**) Western blot of Ephrin-A3 and EhA2. (**E**) Co-IP of NGEF and EphA2. (**F**) Co-IP of Ephrin-A3 and EphA2. (**G**) mRNA level of EphrinA3. One-way ANOVA. **$P < 0.01$, ***$P < 0.001$. (**H**) Protein level of EphrinA3. One-way ANOVA. *$P < 0.05$, **$P < 0.01$, ***$P < 0.001$. (**I**) β-tubulin III staining of neurons. Scale bar: 20 μm. (**J**) Dendritic length between groups. One-way ANOVA. **$P < 0.01$, ***$P < 0.001$

The area of neuro-oncology has attracted significant interest, but there is still a lack of research documenting the existence of nerve fibers in lung cancer cases. This study identified nerve fibers in lung adenocarcinoma specimens using PGP9.5 staining, with the density of these fibers closely associated with the growth of lung adenocarcinoma. Similarly, Jing-Xin Shao et al. observed TH-labeled sympathetic nerve fibers and
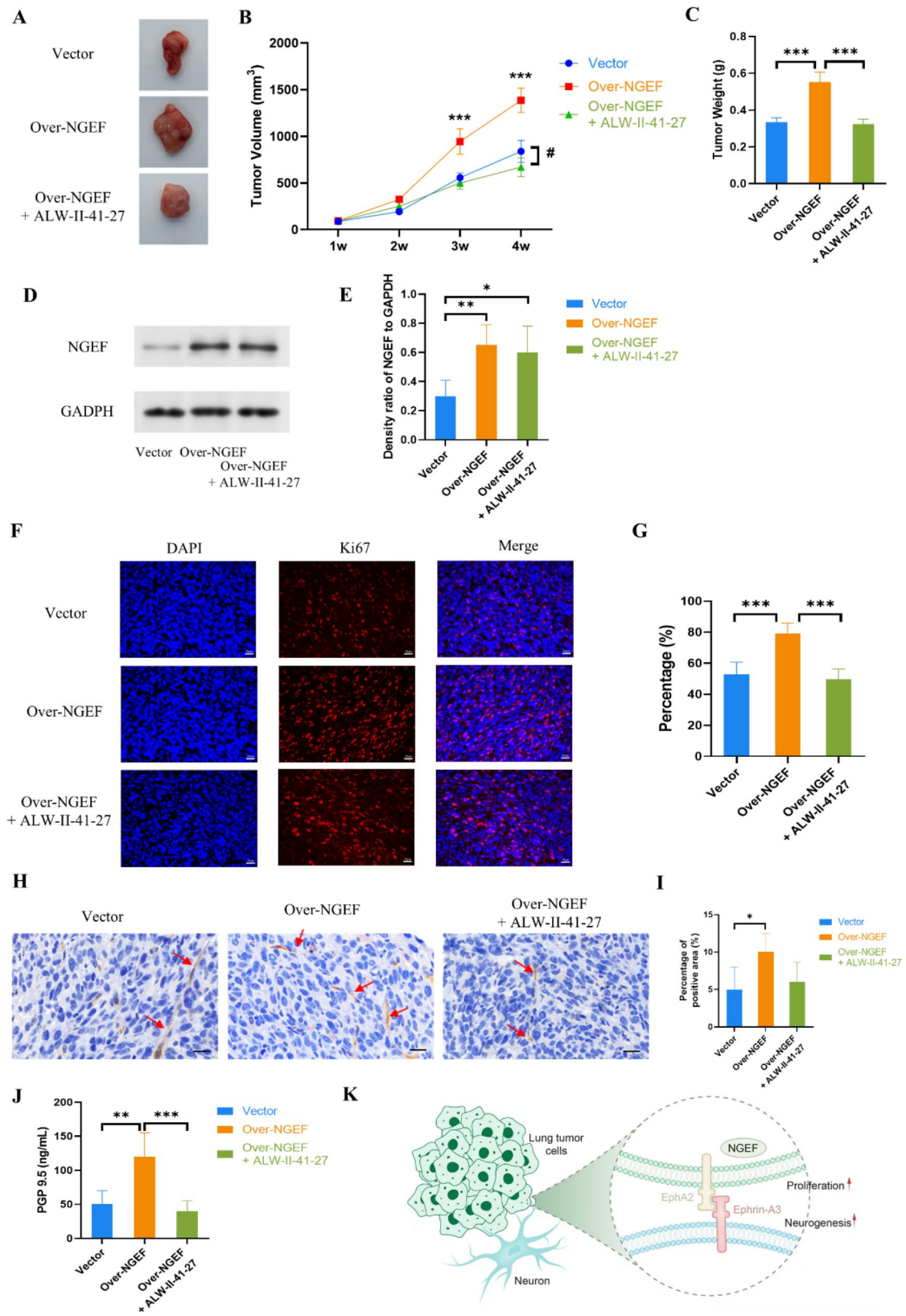
Fig. 6 (See legend on next page.)

(See figure on previous page.)

Fig. 6 NGEF expression promotes the growth of tumor and nerve fibers. (**A**) Xenografts were harvested for imaging and weighing. (**B**&**C**) Tumor weight and volume were calculated at the different time points. Student's t test and Two-way ANOVA. **$P < 0.01$, ***$P < 0.001$ as compared to vector group, #$P < 0.01$ as compared to over-NGEF + ALW-11-41-27 group. (**D**&**E**) Semiquantitative analysis of NGEF expression level by western blot. One-way ANOVA. *$P < 0.05$ and **$P < 0.01$. (**F**&**G**) Ki67 staining and semiquantitative analysis between groups. Scale bar: 20 µm. One-way ANOVA. ***$P < 0.001$. (**H**&**I**) PGP9.5 staining and semiquantitative analysis between groups. Scale bar: 20 µm. *$P < 0.05$. (**J**) PGP 9.5 concentration measured by ELISA and compared between groups. One-way ANOVA. **$P < 0.01$, ***$P < 0.001$. (**K**) Elevated NGEF expression in lung tumor cells promotes the neurogenesis and the proliferation of tumor cells via Ephrin-A3/EphA2 axis

VACHT-immunopositively parasympathetic nerve fibers in human lung adenocarcinoma through immunofluorescence staining, noting a positive correlation between nerve fiber infiltration and the risk of poor prognosis in LUAD patients [4]. Recent findings suggest that neurotransmitters and neuropeptides can promote cancer cell growth and dissemination [24]. For instance, substance P has been implicated in driving malignant progression in breast cancer by sustaining HER2 activation [25], while NGF has been shown to activate cholinergic nerve-mediated signaling in gastric cancer, stimulating stem cell proliferation [26, 27]. Additionally, vagal innervation has been found to contribute to gastric tumorigenesis through M3 receptor-mediated Wnt signaling in gastric cancer stem cells.

To date, few studies have identified the specific factors responsible for promoting nerve fiber growth in lung adenocarcinoma. While previous studies have highlighted proNGF released by prostate cancer cells as a driver of neuronal outgrowth and NGF released by breast cancer cells as a promoter of axonal growth in co-culture with dorsal root ganglia neurons [28, 29], the study by Fangfang Gao et al. revealed that NGF/proNGF do not play a role in stimulating nerve growth in lung cancer [13]. Our co-culture experiments involving tumor and neurons indicate that, despite NGEF's mRNA exhibiting a lower upregulation fold compared to KIF4A and PABPC1, its capacity to facilitate neuronal axon growth was more pronounced. This discrepancy may be attributed to the intracellular localization of KIF4A and PABPC1, as well as the relatively simplified conditions present in the in vitro co-culture environment. To further elucidate the beneficial roles of KIF4A and PABPC1 in neurogenesis associated with lung cancer, it is recommended that future studies involve the direct injection of lung cancer cells overexpressing these proteins into the lungs of murine models, thereby establishing a more representative lung cancer animal model. NGEF belongs to a subset of the Dbl family of guanine nucleotide exchange factors (GEFs) and serves as a direct intermediary between Eph receptors and the Rho-family of GTPases [30]. Through experiments involving NGEF knockout mouse neurons and RNA interference in chick models, Mustafa Sahin et al. determined that NGEF is crucial for normal axonal outgrowth and ephrin-mediated axonal repulsion. Similarly, Chih-Ju Chang et al. illustrated the necessity of NGEF in motor axonal guidance and the role of

Ephrin/Eph signals in determining motor axonal trajectory [31]. Moreover, our research reveals the significant involvement of the Ephrin-A3/EphA2 axis in facilitating neuron extensions induced by NGEF. Recently, Kou et al. and Anderton et al. conducted comprehensive reviews on the involvement of various Ephs/ephrins in lung cancer, highlighting their roles as either promoters or suppressors of tumor growth [32, 33]. Among these, EphA2 has been extensively studied as a target for lung cancer treatment, with the anti-EphA2 antibody DS-8895 undergoing evaluation in a phase I clinical trial involving patients with advanced EPHA2-expressing epithelial NSCLC [34]. Furthermore, the activation of the Ephrin-A3/EphA2 axis has been shown to impact the metabolic characteristics of cells in hepatocellular carcinoma, leading to the enhancement of self-renewal and cancer stemness properties [35]. Although the Eph/ephrin axis plays a crucial role in bidirectional signaling during neural development and the process of nervous system injury and recovery [36], our study did not investigate the potential impact of neurons on lung adenocarcinoma cells through the Ephrin-A3/EphA2 axis.

A recent bioinformatics analysis has indicated an increase in NGEF expression in lung adenocarcinoma tissues compared to normal tissues in TCGA-LUAD and GSE31210 datasets, establishing a significant correlation between NGEF levels and clinical parameters [17]. Our investigation also validated the elevated expression of NGEF in lung adenocarcinoma, showing a positive correlation with tumor size, lymph node metastasis, and reduced overall survival. This suggests the potential of NGEF as a prognostic indicator for LUAD patients. Previous researched have suggested mechanisms through which NGEF influences lung cancer progression and patient outcomes. For instance, Jeeho Kim et al. demonstrated that NGEF activates oncogenic Ras signaling and epidermal growth factor receptor-mediated pathways in lung cancer, leading to increased cancer cell proliferation and tumorigenesis [37, 38]. Our study shows that NGEF facilitates the advancement of lung cancer by stimulating nerve growth and tumor proliferation, indicating that biomaterials aimed at NGEF may be effective in lung cancer treatment. For example, delivering shRNA that inhibits NGEF expression through liposomes targeting lung cancer can lower the levels of NGEF expression [39]. This reduction may lead to decreased neural infiltration and

tumor growth, potentially providing a treatment for lung cancer [40, 41].

The study has several limitations that should be acknowledged. Firstly, while PGP9.5 labeled nerve fibers were identified in lung cancer samples using IHC and ELISA, the specific types of these nerve fibers remain unclear. Recent research has delineated various nerve types present in lung tissue, including sympathetic and parasympathetic nerve fibers [42]. Future investigations could employ immunofluorescence techniques to accurately classify the nerve fiber types in lung cancer tissue. Secondly, the study utilized NGEF overexpression rather than NGEF knockout to assess the impact of NGEF on nerve growth in the subcutaneous tumor formation model. This approach may result in an underestimation of NGEF's influence on nerve axonal growth. Lastly, it is important to note that the expression of nerve fibers in human and animal specimens may differ. Consequently, findings from animal experiments may only partially elucidate the outcomes of bioinformatics analyses.

Conclusion

This research revealed that NGEF plays a role in promoting neurite outgrowth and cancer cell proliferation in lung adenocarcinoma by acting through the Ephrin-A3/EphA2 axis. The study first confirmed the existence of nerve fibers in lung cancer using samples from clinical cases. Subsequent bioinformatic analysis and laboratory experiments indicated a positive association between heightened NGEF levels and larger tumor size, greater nerve fiber density, and the involvement of Ephrin-A3/EphA2 axis. These results provide a new insight into potential approaches for controlling the progression of lung adenocarcinoma.

Abbreviations

LUAD   Lung adenocarcinoma
NGEF   Neuronal guanine nucleotide exchange factor
TCGA   Cancer genome atlas
DEGs   Differentially expressed genes
GEO   Gene expression omnibus
HPA   Human protein atlas
GSEA   Gene set enrichment analysis
qPCR   Quantitative polymerase chain reaction

Supplementary Information

The online version contains supplementary material available at https://doi.or g/10.1186/s12967-025-06233-8.

Supplementary Material 1

Declarations

Ethics approval and consent to participate
This study was approved by the Ethics Committee of Shanghai Pulmonary Hospital Affiliated Tongji University (approval no: K21-111Y) and Bestcell Model Biological Center (BSMS 2024-01-22 A).

Consent for publication
Not applicable.

Competing interests
The authors declare no competing interests.

Author details
¹Department of Thoracic Surgery, Shanghai Pulmonary Hospital, Tongji University School of Medicine, Shanghai, People's Republic of China

References
1. Siegel RL, Miller KD, Fuchs HE, Jemal A, Cancer Statistics. 2021. CA Cancer J Clin. 2021;71(1):7–33.
2. Fong KM, Rosenthal A, Giroux DJ, Nishimura KK, Erasmus J, Lievens Y, et al. The International Association for the study of Lung Cancer Staging Project for Lung Cancer: proposals for the revision of the M descriptors in the Forthcoming Ninth Edition of the TNM classification for Lung Cancer. J Thorac Oncol. 2024;19(5):786–802.
3. Wang X, Yang J, Gao X. Identification of key genes associated with lung adenocarcinoma by bioinformatics analysis. Sci Prog. 2021;104(1):36850421997276.
4. Shao JX, Wang B, Yao YN, Pan ZJ, Shen Q, Zhou JY. Autonomic nervous infiltration positively correlates with pathological risk grading and poor prognosis in patients with lung adenocarcinoma. Thorac Cancer. 2016;7(5):588–98.
5. Regan JL, Schumacher D, Staudte S, Steffen A, Lesche R, Toedling J, et al. Identification of a neural development gene expression signature in colon cancer stem cells reveals a role for EGR2 in tumorigenesis. iScience. 2022;25(7):104498.
6. Tan X, Sivakumar S, Bednarsch J, Wiltberger G, Kather JN, Niehues J, et al. Nerve fibers in the tumor microenvironment in neurotropic cancer-pancreatic cancer and cholangiocarcinoma. Oncogene. 2021;40(5):899–908.
7. Magnon C, Hall SJ, Lin J, Xue X, Gerber L, Freedland SJ, et al. Autonomic nerve development contributes to prostate cancer progression. Science. 2013;341(6142):1236361.
8. Akoun GM, Scarna HM, Milleron BJ, Bénichou MP, Herman DP. Serum neuron-specific enolase. A marker for disease extent and response to therapy for small-cell lung cancer. Chest. 1985;87(1):39–43.
9. Huang Z, Xu D, Zhang F, Ying Y, Song L. Pro-gastrin-releasing peptide and neuron-specific enolase: useful predictors of response to chemotherapy and survival in patients with small cell lung cancer. Clin Transl Oncol. 2016;18(10):1019–25.
10. Amit M, Takahashi H, Dragomir MP, Lindemann A, Gleber-Netto FO, Pickering CR, et al. Loss of p53 drives neuron reprogramming in head and neck cancer. Nature. 2020;578(7795):449–54.

11. Monje M, Borniger JC, D'Silva NJ, Deneen B, Dirks PB, Fattahi F, et al. Roadmap for the Emerging Field of Cancer Neuroscience. Cell. 2020;181(2):219–22.

12. Darragh LB, Nguyen A, Pham TT, Idlett-Ali S, Knitz MW, Gadwa J, et al. Sensory nerve release of CGRP increases tumor growth in HNSCC by suppressing TILs. Med. 2024;5(3):254–e708.

13. Gao F, Griffin N, Faulkner S, Rowe CW, Williams L, Roselli S, et al. The neurotrophic tyrosine kinase receptor TrkA and its ligand NGF are increased in squamous cell carcinomas of the lung. Sci Rep. 2018;8(1):8135.

14. Bian Z, Fan R, Xie L. A Novel cuproptosis-related prognostic gene signature and validation of Differential expression in Clear Cell Renal Cell Carcinoma. Genes (Basel). 2022;13(5).

15. Zhao H, Jiang R, Feng Z, Wang X, Zhang C. Transcription factor LHX9 (LIM Homeobox 9) enhances pyruvate kinase PKM2 activity to induce glycolytic metabolic reprogramming in cancer stem cells, promoting gastric cancer progression. J Transl Med. 2023;21(1):833.

16. Jung WY, Min KW, Oh YH. Increased VEGF-A in solid type of lung adenocarcinoma reduces the patients' survival. Sci Rep. 2021;11(1):1321.

17. Chen X, Zhang T, He YQ, Miao TW, Yin J, Ding Q, et al. NGEF is a potential prognostic biomarker and could serve as an indicator for immunotherapy and chemotherapy in lung adenocarcinoma. BMC Pulm Med. 2024;24(1):248.

18. Ulmann L, Rodeau JL, Danoux L, Contet-Audonneau JL, Pauly G, Schlichter R. Dehydroepiandrosterone and neurotrophins favor axonal growth in a sensory neuron-keratinocyte coculture model. Neuroscience. 2009;159(2):514–25.

19. Hansson ML, Chatterjee U, Francis J, Arndt T, Broman C, Johansson J, et al. Artificial spider silk supports and guides neurite extension in vitro. Faseb j. 2021;35(11):e21896.

20. Chen J, Liu A, Wang Z, Wang B, Chai X, Lu W, et al. LINC00173.v1 promotes angiogenesis and progression of lung squamous cell carcinoma by sponging mir-511-5p to regulate VEGFA expression. Mol Cancer. 2020;19(1):98.

21. Mi J, Xu J, Yao H, Li X, Tong W, Li Y, et al. Calcitonin gene-related peptide enhances distraction osteogenesis by increasing angiogenesis. Tissue Eng Part A. 2021;27(1–2):87–102.

22. Mi J, Xu JK, Yao Z, Yao H, Li Y, He X, et al. Implantable Electrical stimulation at dorsal Root ganglions accelerates osteoporotic fracture Healing via Calcitonin Gene-related peptide. Adv Sci (Weinh). 2022;9(1):e2103005.

23. He Q, Qu M, Shen T, Xu Y, Luo J, Tan D, et al. Suppression of VEGFD expression by S-nitrosylation promotes the development of lung adenocarcinoma. J Exp Clin Cancer Res. 2022;41(1):239.

24. Erin N, Shurin GV, Baraldi JH, Shurin MR. Regulation of carcinogenesis by sensory neurons and neuromediators. Cancers (Basel). 2022;14(9).

25. Garcia-Recio S, Fuster G, Fernandez-Nogueira P, Pastor-Arroyo EM, Park SY, Mayordomo C, et al. Substance P autocrine signaling contributes to persistent HER2 activation that drives malignant progression and drug resistance in breast cancer. Cancer Res. 2013;73(21):6424–34.

26. Zhao CM, Hayakawa Y, Kodama Y, Muthupalani S, Westphalen CB, Andersen GT, et al. Denervation suppresses gastric tumorigenesis. Sci Transl Med. 2014;6(250):250ra115.

27. Hayakawa Y, Sakitani K, Konishi M, Asfaha S, Niikura R, Tomita H, et al. Nerve growth factor promotes gastric tumorigenesis through aberrant Cholinergic Signaling. Cancer Cell. 2017;31(1):21–34.

28. Mazaki AI, Yamauchi K, Orita S, Inage K, Suzuki M, Fujimoto K, et al. Nerve growth factor in breast Cancer cells promotes Axonal Growth and expression of calcitonin gene-related peptide in a rat model of spinal metastasis. Anticancer Res. 2022;42(1):581–7.

29. Pundavela J, Demont Y, Jobling P, Lincz LF, Roselli S, Thorne RF, et al. ProNGF correlates with Gleason score and is a potential driver of nerve infiltration in prostate cancer. Am J Pathol. 2014;184(12):3156–62.

30. Kim K, Lee SA, Park D. Emerging roles of ephexins in Physiology and Disease. Cells. 2019;8(2).

31. Chang CJ, Chang MY, Chou SY, Huang CC, Chuang JY, Hsu TI, et al. Ephexin1 is required for eph-mediated limb trajectory of spinal motor axons. J Neurosci. 2018;38(8):2043–56.

32. Kou CJ, Kandpal RP. Differential expression patterns of eph receptors and ephrin ligands in human cancers. Biomed Res Int. 2018;2018:7390104.

33. Anderton M, van der Meulen E, Blumenthal MJ, Schäfer G. The role of the eph receptor family in Tumorigenesis. Cancers (Basel). 2021;13(2).

34. Gan HK, Parakh S, Lee FT, Tebbutt NC, Ameratunga M, Lee ST, et al. A phase 1 safety and bioimaging trial of antibody DS-8895a against EphA2 in patients with advanced or metastatic EphA2 positive cancers. Invest New Drugs. 2022;40(4):747–55.

35. Husain A, Chiu YT, Sze KM, Ho DW, Tsui YM, Suarez EMS, et al. Ephrin-A3/EphA2 axis regulates cellular metabolic plasticity to enhance cancer stemness in hypoxic hepatocellular carcinoma. J Hepatol. 2022;77(2):383–96.

36. Yang JS, Wei HX, Chen PP, Wu G. Roles of Eph/ephrin bidirectional signaling in central nervous system injury and recovery. Exp Ther Med. 2018;15(3):2219–27.

37. Kim J, Chang IY, You HJ. Interactions between EGFR and EphA2 promote tumorigenesis through the action of Ephexin1. Cell Death Dis. 2022;13(6):528.

38. Kim J, Jeon YJ, Lim SC, Ryu J, Lee JH, Chang IY, et al. Akt-mediated Ephexin1-Ras interaction promotes oncogenic ras signaling and colorectal and lung cancer cell proliferation. Cell Death Dis. 2021;12(11):1013.

39. Beigi A, Naghib SM, Matini A, Tajabadi M, Mozafari MR. Lipid-based nanocarriers for targeted gene delivery in Lung Cancer Therapy: exploring a Novel Therapeutic paradigm. Curr Gene Ther. 2025;25(2):92–112.

40. Rosic G. Cancer signaling, cell/gene therapy, diagnosis and role of nanobiomaterials. Adv Biology Earth Sci. 2024;9:11–34.

41. Montazersaheb S, Eftekhari A, Shafaroodi A, Tavakoli S, Jafari S, Baran A et al. Green-synthesized silver nanoparticles from peel extract of pumpkin as a potent radiosensitizer against triple-negative breast cancer (TNBC). Cancer Nanotechnol. 2024;15.

42. Kim SH, Patil MJ, Hadley SH, Bahia PK, Butler SG, Madaram M et al. Mapping of the sensory innervation of the mouse lung by specific vagal and dorsal Root Ganglion neuronal subsets. eNeuro. 2022;9(2).

Publisher's note